Abdominal Radiology (2022) 47:3971–3985
https://doi.org/10.1007/s00261-022-03430-7

SPECIAL SECTION: NEUROENDOCRINE

Qualitative imaging features of pancreatic neuroendocrine neoplasms predict histopathologic characteristics including tumor grade and patient outcome

Motoyo Yano[1,2] · Anup S. Shetty[1] · Greg A. Williams[3] · Samantha Lancia[4] · Nikolaos A. Trikalinos[5] · Chet W. Hammill[3] · William G. Hawkins[3] · Amber Salter[4] · Deyali Chatterjee[6,7]

Received: 30 November 2021 / Revised: 22 January 2022 / Accepted: 25 January 2022 / Published online: 15 February 2022

Abstract

Objectives To identify PanNEN imaging features associated with tumor grade and aggressive histopathological features.

Methods Associations between histopathological and imaging features of resected PanNEN were retrospectively tested. Histopathologic features included WHO grade, lymphovascular invasion (LVI), growth pattern (infiltrative, circumscribed), and intratumoral fibrosis (mature, immature). Imaging features included size, degree/uniformity of enhancement, progressive enhancement, contour, infiltrative appearance (infiltrative$_{im}$), calcifications, cystic components, tumor thrombus, vascular occlusion (VO), duct dilatation, and atrophy. Multinomial logistic regression analyses evaluated the magnitude of associations. Association of variables with outcome was assessed using Cox-proportional hazards regression.

Results 133 patients were included. 3 imaging features (infiltrative$_{im}$, ill-defined contour [contour$_{ill}$], and VO) were associated with all histopathologic parameters and poor outcome. Increase in grade increased odds of contour$_{ill}$ by 15.6 times ($p=0.0001$, 95% CI 3.8–64.4). PanNEN with VO were 51.1 times ($p=0.0002$, 6.5–398.6) more likely to demonstrate LVI. For PanNEN with contour$_{ill}$, infiltrative growth pattern was 51.3 times ($p<0.0001$, 9.1–288.4), and fibrosis was 14 times ($p=0.0065$, 2.1–93.7) more likely. Contour$_{ill}$ was associated with decreased recurrence-free survival ($p=0.0003$, HR 18.29, 3.83–87.3) and VO ($p=0.0004$, HR6.08, 2.22–16.68) with decreased overall survival.

Conclusions Infiltrative$_{im}$, contour$_{ill}$, and VO on imaging are associated with higher grade/histopathological parameters linked to tumor aggression, and poor outcome.

Keywords Pancreatic neuroendocrine neoplasm · WHO grade · Imaging · CT · MRI · Patient outcome

✉ Motoyo Yano
yano.motoyo@mayo.edu

[1] Mallinckrodt Institute of Radiology, Washington University School of Medicine, 510 S. Kingshighway Blvd. CB 8131, Saint Louis, MO 63110, USA

[2] Present Address: Department of Radiology, Mayo Clinic Arizona, 13400 E. Shea Blvd, Scottsdale, AZ 85259, USA

[3] Department of Surgery, Washington University School of Medicine, St Louis, MO, USA

[4] Present Address: Section on Statistical Planning and Analysis, Department of Neurology, UT Southwestern Medical Center, Dallas, TX, USA

[5] Division of Medical Oncology, Department of Internal Medicine, Washington University School of Medicine and Siteman Cancer Center, MO, St Louis, USA

[6] Department of Pathology, Washington University School of Medicine, St Louis, MO, USA

[7] Present Address: Department of Pathology, University of Texas MD Anderson Cancer Center, Houston, TX, USA

Introduction

Pancreatic neuroendocrine neoplasms (PanNEN) demonstrate variable biological behavior. This is reflected in part by histopathologic grading according to the WHO 2019 classification system which categorizes PanNEN by tumor differentiation and mitotic activity/ki-67 index [1]. By this system, well-differentiated grade 1 tumors are the most indolent, followed by grade 2 and grade 3 tumors. Besides tumor grade, other histopathological variables such as lymphovascular invasion (LVI), infiltrative growth pattern, and intratumoral fibrosis have been linked to tumor recurrence and decreased survival [2, 3].

Tumor grade and other histopathologic features may be difficult to adequately assess with the limited tissue available from biopsy specimens, especially since PanNEN may show tumor heterogeneity [4, 5]. There is accumulating data emerging in the review literature showing that the clinical behavior of PanNEN may be reflected in their imaging appearance, with grade 1 tumors manifesting with round, well-circumscribed margins and hyperenhancement [6]. Most of the early literature focused on enhancement characteristics [7–9] and relatively less on the morphologic features of the tumor until recently.

Routine pre-procedural imaging with CT and MRI provides an opportunity to gain information about the nature of the tumor before tissue diagnosis and surgical management. Our objective in this study was to determine whether prognostic histopathological variables, specifically WHO grade, LVI, tumoral growth pattern, and intratumoral fibrosis, have qualitative imaging correlates that can be readily characterized on preoperative imaging.

Materials and methods

This was a HIPAA-compliant, single institution, IRB approved, study populated from a search of a prospectively maintained surgical database from 2000–2018. Informed consent was waived. Records were excluded if preoperative CT or MRI was not available: Imaging prior to 2006 was not available in the institutional Picture Archiving and Communication System (PACS), so the population essentially consisted of resected cases from 2006–2018. The imaging modality, and if CT, the phases of contrast performed, was recorded. The scanning parameters for pancreas protocol CT have previously been published [10]. Cases were excluded if CT or MRI performed at an outside institution were not available for review. Records were also excluded if pathology slides were unavailable, if the NEN was not pancreatic, if there were multiple PanNEN, or if a pediatric patient. Demographic variables from the surgical database include age at diagnosis, sex, race, body mass index at diagnosis, recurrence-free survival (RFS) time, and overall survival (OS) time.

Tumors were assessed histopathologically by a gastrointestinal pathologist for four parameters: WHO 2019 criteria for classification and grade, lymphovascular invasion, growth pattern (circumscribed or infiltrative), and intratumoral fibrosis (no significant fibrosis, mature fibrosis [MF], or immature fibrosis [IMF]). The latter three parameters are described in detail elsewhere [2]. Briefly, these histologic assessments were made on routine H&E sections. Lymphovascular invasion was considered when tumor cells were identified in vascular spaces at the periphery of, or away from the tumor. If more than 10% of the tumor periphery showed irregular infiltration greater than 0.1 cm into adjacent stroma, the growth pattern was classified as infiltrative, otherwise circumscribed. A tumor was considered significant for intratumoral fibrosis if at least 10% of the tumor area showed a fibrous stroma. If the appearance of the stroma was dense collagenous, hypocellular, or hyalinized, it was considered as MF. The presence of myxoid stroma with plump fibroblasts, involving at least 20% of the area of fibrosis, was classified as IMF. If histopathology slides were insufficient to assess a particular histopathologic parameter, then that parameter was excluded (Fig. 1).

Prior to assessment, imaging features were reviewed (Figs. 2, 3, 4) by two abdominal radiologists (ASS and MY) with 5 and 7 years, respectively, of post-fellowship experience at the time of review. Blinded to the pathology analysis, images were assessed independently and discrepancies were resolved by re-review in person after 2 months. Enhancement of the solid portion of tumor was categorized in several ways. Uniformity of enhancement was categorized as homogeneous or heterogeneous (Fig. 2). The degree of enhancement ($enhancement_{deg}$) was characterized as hyper, hypo, or isoenhancement relative to the pancreas in the pancreatic parenchymal phase of contrast when available, and if not available, was characterized in the portal venous phase. If heterogeneously enhancing, the $enhancement_{deg}$ was characterized by its most hypoenhancing area ("cold spot" analysis [10]). Progressive enhancement ($enhancement_{prog}$), defined as tumor showing increasing enhancement relative to the pancreas on later phases, was only assessed on multiphase exams.

Tumor contour was an assessment of external margin as rounded, lobulated, or ill-defined ($contour_{ill}$; Fig. 3). A tumor characterized as having infiltrative imaging appearance ($infiltrative_{im}$) obliterated fat planes or invaded adjacent organs or vessels (Fig. 4). Upstream pancreatic duct (PD) dilatation and upstream parenchymal atrophy were assessed for all tumors except those in the distalmost tail. Calcifications were assessed by CT. The presence of cystic components was defined as fluid intensity on T2 weighted

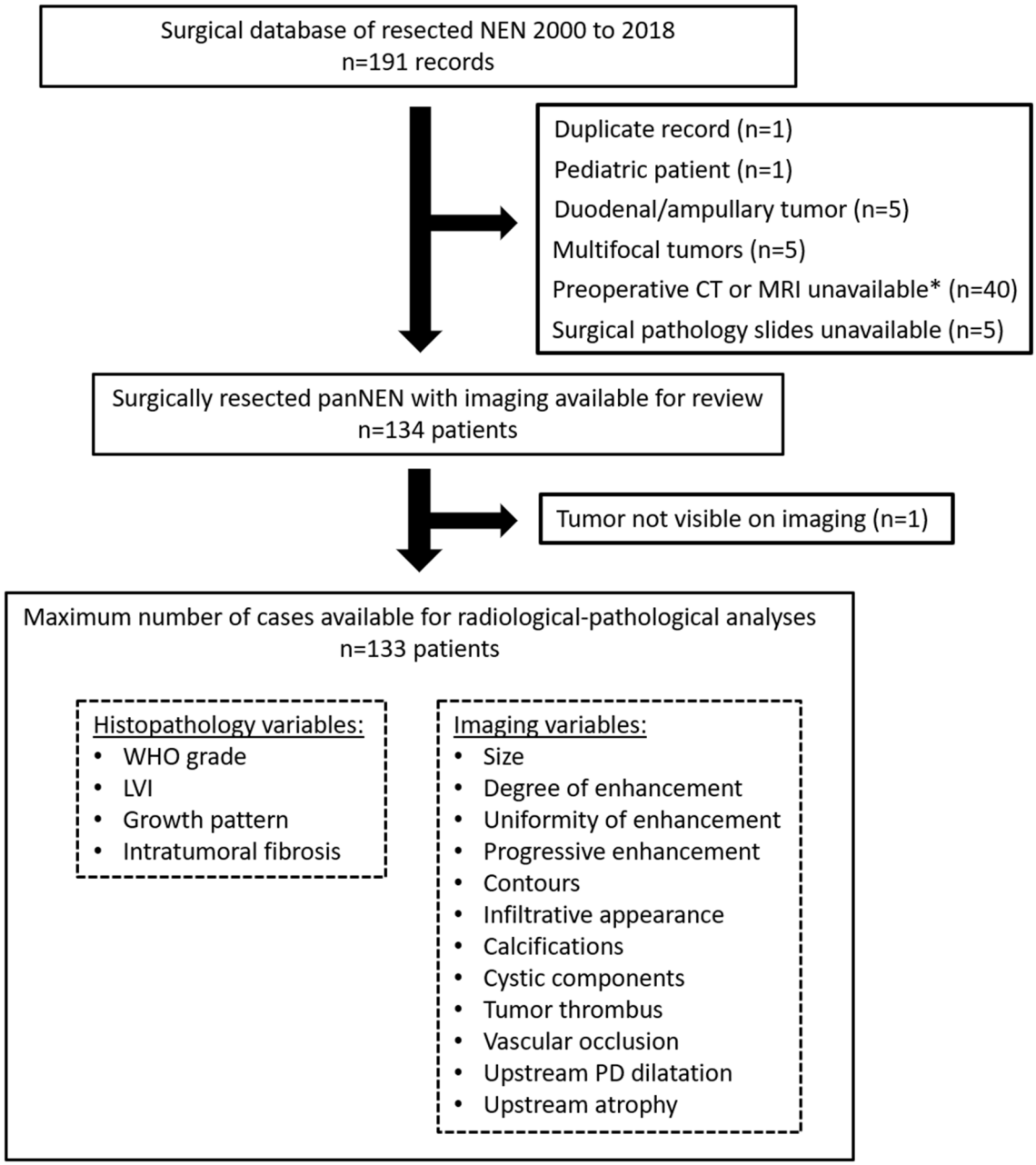

Fig. 1 Flow diagram shows exclusions applied to obtain the study population. *WHO* World Health Organization, *LVI* lymphovascular invasion, *PD* pancreatic duct. *Images obtained prior to 2006 were not available in the institutional Picture Archiving and Communication System (PACS). Therefore, no cases resected prior to 2006 were included

MR and/or hypodensity without increase in attenuation on multiphasic CT. Vascular occlusion (VO) was present when a vessel was obliterated or attenuated in caliber with or without the presence of collateral veins (Fig. 4B). Tumor thrombus was defined as a vascular filling defect contiguous with tumor. Occlusive tumor thrombus was also categorized as VO. Tumor size (greatest axial dimension) was measured by a single radiologist (initials blinded). If an imaging feature could not be assessed based on the images available that feature was not included in analysis.

Descriptive statistics were used to summarize patient characteristics. Continuous data are summarized using mean (standard deviation [SD]) and median (IQR). Categorical variables are summarized using frequencies (%n). Kruskall-Wallis and Chi-Square tests, and Fisher's Exact Tests (when appropriate) were performed to evaluate associations with imaging variables. Post-hoc group comparisons

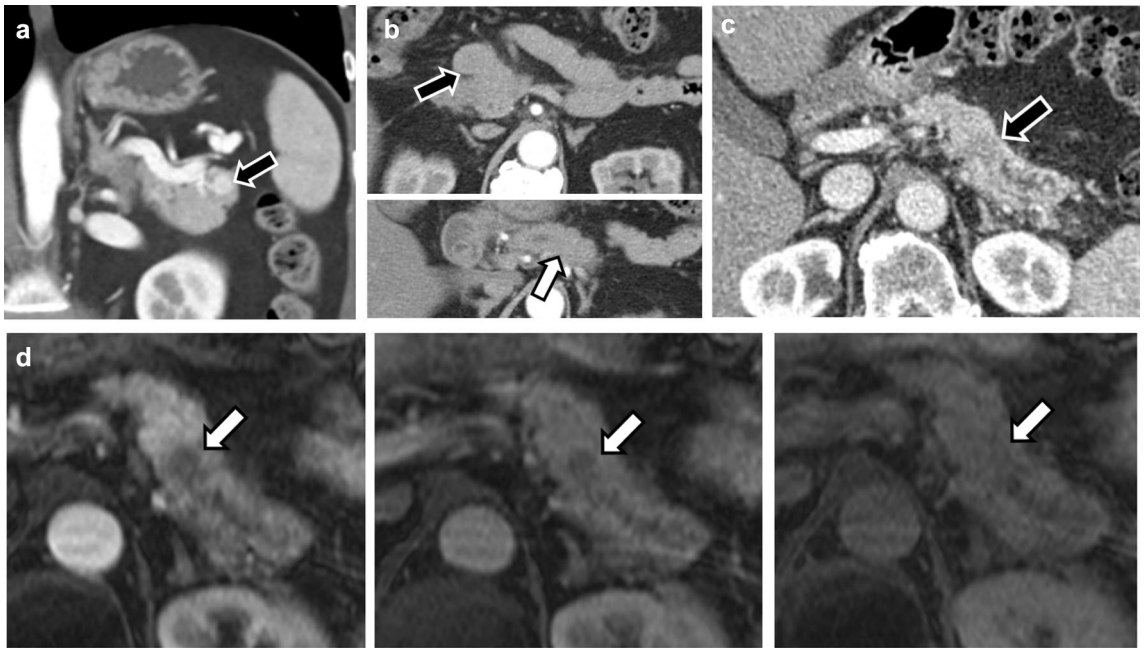

Fig. 2 **a**–**c** Degree of enhancement was categorized as hyperenhancement, isoenhancement, and hypoenhancement in the pancreatic parenchymal phase if available, and if not, was assessed in the portal venous phase. **a** On coronal reformatted contrast-enhanced CT image, a NET in the tail of the pancreas demonstrates hyperenhancement relative to the pancreas in the pancreatic parenchymal phase. It is also rounded in contour and has uniform, homogeneous enhancement. **b**. An isoenhancing lesion is by definition difficult to detect as it enhances similar to the pancreatic parenchyma. In this example, the tumor in the pancreatic head is detected due to its round, exophytic nature from the pancreatic head (black arrow). The enhancement of the upstream pancreatic body (white arrow) is shown in the bottom panel for comparison. **c** Hypoenhancing tumors (black arrow) enhance less than the adjacent parenchyma. This tumor in the pancreatic body/tail junction also demonstrates upstream ductal dilatation. **d** Progressive enhancement was assessed only on multiphase examinations. For progressive enhancement to be present, the attenuation or intensity of the tumor relative to the pancreas increases over time. This pancreatic body/tail junction tumor (white arrow) shows moderate hypoenhancement relative to the pancreas in the pancreatic parenchymal phase (left), followed by mild hypoenhancement (center) and isoenhancement in the venous phase of contrast (right)

for associations between imaging predictors and pathology were conducted when the omnibus test was statistically significant. Univariate binomial and multinomial logistic regression analyses were used for chi-square test and ordinal logistic regression was used for analyses of tumor grade. The odds ratios (OR) and 95% confidence interval (CI) were reported. Statistical significance was set at the 0.05 level.

OS was calculated from the date of diagnosis to the date of last follow-up or the date of death. RFS was calculated from the date of diagnosis to the last follow-up visit or the event of disease recurrence. Patients who did not experience the event of interest were censored at their last date of follow-up. For significant predictors of survival, survival curves were generated using the Kaplan–Meier method. Univariate and multivariable Cox-proportional hazard models were constructed to evaluate parameters of pathology, imaging and the combination of pathology, and imaging as predictors of survival. Covariate selection for each of the three multivariable models used a stepwise selection method with $p < 0.2$ entry criteria for inclusion. Missing data in the multivariable models were set to the reference level for that variable. The hazard ratio (HR) and 95% CI were reported. All tests were two sided. All analyses were conducted in SAS version 9.4 (SAS, Cary, NC).

Results

Patient population

The surgical database yielded 191 records for surgically managed PanNEN. After 58 exclusions, most due to lack of preoperative imaging ($n = 40$; Fig. 1), there were 133 PanNEN, 56% men and mean age of 58.2 years (Table 1). Approximately three quarters of the population had a preoperative CT, while the remainder had MR. Most CTs were pancreas protocol (n = 69/101). 24% had a preoperative MR, approximately half of which also had a CT. 18% of patients had tumor recurrence (median RFS of 31 months). 12% of patients were deceased (median OS of 38 months).

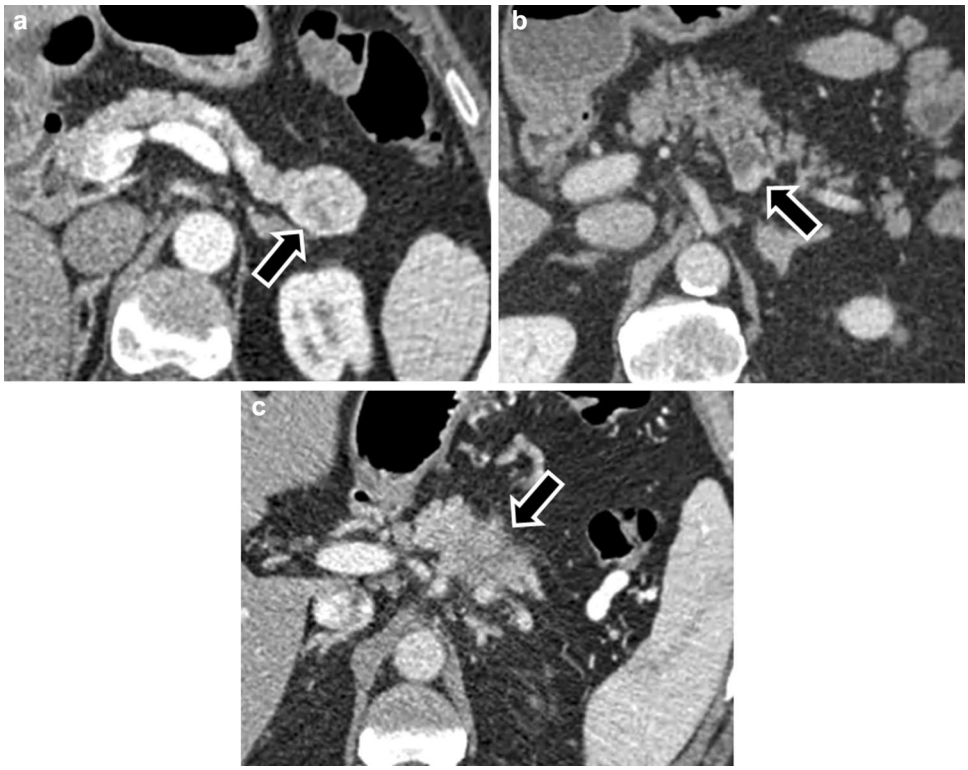

Fig. 3 **a**, **b** A rounded contour to the tumor was defined as minimal contour undulation with a generally spherical or ovoid shape. This heterogeneously enhancing mass in the tail (black arrow) is rounded in contour. **b** A lobulated contour is defined by undulations in the contour of the tumor. In this partially cystic neuroendocrine tumor (black arrow), the external contour of the posterior aspect of the tumor is lobulated. **c** A tumor with an ill-defined contour has tumor margins which are difficult to delineate. This neuroendocrine tumor at the body/tail junction (arrow) has margins that are difficult to discriminate from the adjacent pancreas

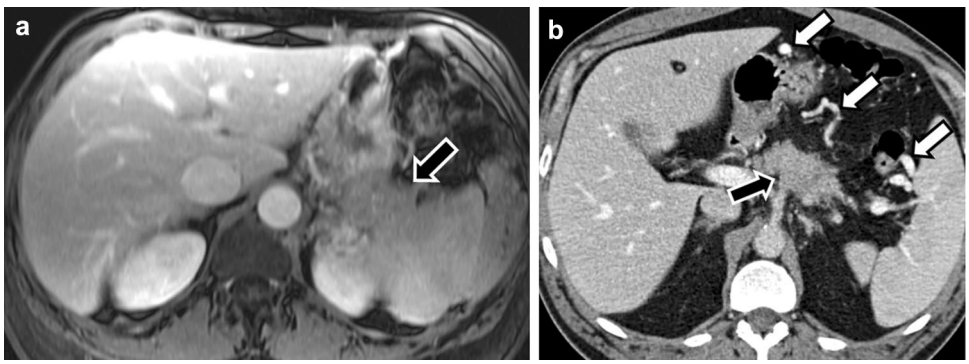

Fig. 4 **a**, **b** Infiltrative tumors are defined as tumors which obliterate fat planes with or invade adjacent organs or vessels. Two imaging examples are shown. **a** On this axial post-contrast T1 fat-saturated MR image through the pancreatic tail mass, the tumor (black arrow) invades the splenic hilum, obliterating the fat and vessels in the splenic hilum. **b** Axial contrast-enhanced CT shows a pancreatic body mass (black arrow) which has engulfed splenic vessels, including the splenic vein, resulting in vascular occlusion and venous collaterals in the left upper quadrant (white arrows)

WHO grade

One tumor in the study population was poorly differentiated. Of the 119 well-differentiated tumors available for grading, there were 47 (39%) grade 1, 64 (54%) grade 2, and 8 (7%) grade 3 tumors (Table 2). Median tumor size was 2.4 cm (IQR 1.8–3.9 cm). There was no significant difference in size between tumor grades ($p = 0.051$).

WHO grade (Table 2) was significantly associated with enhancement$_{deg}$ ($p < 0.001$), enhancement$_{prog}$ ($p < 0.001$), contours ($p = 0.001$), infiltrative$_{im}$ ($p < 0.001$), VO ($p < 0.001$), PD dilatation ($p = 0.005$), and upstream atrophy ($p = 0.04$). For each increase in grade from WHO grade 1, PanNEN were 7 times more likely ($p = 0.0002$, 95% CI 2.5–19.1) to be hypoenhancing than hyperenhancing, 6.2 times ($p = 0.0008$, 95% CI 2.1–17.8) more likely to demonstrate enhancement$_{prog}$, 15.6 times ($p = 0.0001$, 95% CI 3.8–64.4) more likely to have contour$_{ill}$, 9 times ($p = 0.0003$, 95%CI 2.7–29.7) more likely to have infiltrative$_{im}$, 12.5 times ($p = 0.0001$, 95% CI 3.5–44.6) more likely to show

Table 1 Patient data

Factor	Total ($n=133$)
Age at diagnosis	58.2 ± 14.0
Race*	
Caucasian	112 (84.8)
African American	17 (12.9)
Asian	3 (2.3)
Sex	
Male	75 (56.4)
Female	58 (43.6)
BMI at Diagnosis*	30.0 ± 7.6
Imaging modality	
CT	101 (75.9)
Pancreas protocol (noncontrast, arterial, PV phases)	70
Noncontrast only	3
PV phase only	17
PV phase and additional post-contrast phase[a]	11
MR	32 (24.0)
Dynamic post-contrast imaging	31
Preoperative CT also available	17
Post-operative tumor recurrence?	
No	109 (82.0)
Yes	24 (18.0)
Recurrence-Free Survival Time (in months)*	31.5 [15.0,67.5]
Is the patient deceased?	
No	117 (88.0)
Yes	16 (12.0)
Overall Survival Time (in months)	38.0 [24.0,82.0]

[a]additional post-contrast phases include arterial or delayed phases, without inclusion of noncontrast images in the exam

*Data not available for all subjects. Missing values: Race = 1, BMI at Diagnosis = 3, Recurrence-Free Survival Time = 1

Values presented as Mean ± SD, Median [P25, P75], Median (min, max) or N (column %)

VO, and 4.7 times ($p=0.02$, 95% CI 1.3–17.7) more likely to show PD dilatation (Table 3).

LVI

Lymphovascular invasion (LVI) was present in 48 of 131 tumors (36.6%). The presence of LVI on histopathological assessment (Table 4) was significantly associated with the following variables: size ($p=0.001$), $\text{enhancement}_{\text{deg}}$ ($p=0.03$), uniformity of enhancement ($p<0.001$), $\text{enhancement}_{\text{prog}}$ ($p=0.001$), contours ($p<0.001$), $\text{infiltrative}_{\text{im}}$ ($p<0.001$), cystic components ($p=0.005$), VO ($p<0.001$) PD dilatation ($p=0.007$), and upstream atrophy ($p<0.001$). The likelihood of LVI was increased 1.2 times ($p=0.005$, 95%CI 1.1–1.4) for each 1 cm increase in tumor size, 3 times ($p=0.0135$, 95% CI 1.3–7.3) for hypoenhancing tumors, 3.8 times ($p=0.0008$, 95%CI 1.8–8.6) for heterogeneously enhancing tumors, 4.5 times ($p=0.002$, 95% CI 1.7–11.3) for $\text{enhancement}_{\text{prog}}$, 18 times ($p<0.001$, 95% CI 4.4–73.8) for $\text{contour}_{\text{ill}}$, 25.9 times ($p<0.001$, 95% CI 5.7–118.1) for $\text{infiltrative}_{\text{im}}$, 51.1 times ($p=0.0002$, 95% CI 6.5–398.6) for VO, 4.6 times ($p=0.01$, 95% CI 1.4–15.3) for PD dilation, and 7.4 times ($p=0.0003$, 95% CI 2.5–21.8) for atrophy. The presence of cystic components was 3.8 times ($p=0.007$, 95% CI 1.5–10.2) less likely to be associated with LVI (Table 3).

Growth pattern

An infiltrative rather than circumscribed growth pattern on histopathology was present in 24 of 120 (20%) tumors. An infiltrative growth pattern (Table 5) was significantly associated with the following: $\text{enhancement}_{\text{deg}}$ ($p=0.006$), $\text{enhancement}_{\text{prog}}$ ($p<0.001$), contours ($p<0.001$), $\text{infiltrative}_{\text{im}}$ ($p<0.001$), VO ($p<0.001$), PD dilatation ($p<0.001$), and upstream atrophy ($p=0.02$). The odds of an infiltrative rather than circumscribed growth pattern is 5.6 times ($p=0.003$, 95%CI 1.8–17.3) more likely for hypoenhancing tumors, 7.7 times ($p=0.0001$, 95%CI 2.7–21.8) more likely for tumors with $\text{enhancement}_{\text{prog}}$, 51.3 times ($p<0.0001$, 95%CI 9.1–288.4) more likely for $\text{contour}_{\text{ill}}$, 17.3 times ($p<0.0001$, 95%CI 5.5–54.9) more likely with $\text{infiltrative}_{\text{im}}$, 16.9 times ($p<0.0001$, 95%CI 5.3–53.7) more likely with VO, 7.4 times ($p=0.003$, 95%CI 2–27.5) more likely with PD dilatation, and 4.4 times ($p=0.02$, 95%CI 1.3–15) more likely with atrophy.

Intratumoral fibrosis

Of the 120 cases available to assess fibrosis, 70 tumors demonstrated no fibrosis, 36 MF, and 14 IMF (Table 6). Significant associations were found for $\text{enhancement}_{\text{deg}}$ ($p=0.006$), $\text{enhancement}_{\text{prog}}$ ($p=0.048$), contours ($p=0.01$), $\text{infiltrative}_{\text{im}}$ ($p<0.001$), calcifications ($p=0.03$), cystic components ($p=0.01$), VO ($p=0.04$), PD dilatation ($p<0.001$), and atrophy ($p=0.004$).

Hypoenhancing tumors were 11.5 times ($p=0.004$, 95% CI 2.2–60.3) more likely to be associated with MF (Table 7). $\text{Enhancement}_{\text{prog}}$ was 4.8 times ($p=0.02$, 95% CI 1.3–18) more likely to be associated with IMF.

$\text{Contour}_{\text{ill}}$ was 10.5 times ($p=0.006$, 95%CI 1.9–56.6) and 14 times ($p=0.007$, 95%CI 2.1–93.7) more likely than rounded contours and 6.3 times ($p=0.04$, 95% CI 1.1–34.3) and 12.5 times ($p=0.01$, 95% CI 1.7–92.2) more likely than lobulated contours to be associated with MF and IMF, respectively (Table 7). $\text{Infiltrative}_{\text{im}}$ tumors were 5.6 times ($p=0.007$, 95%CI 1.6–19.9) more likely to be associated with MF and 12.2 times ($p=0.0008$, 95% CI 2.8–52.6) more likely to be associated with IMF. Calcifications and

Table 2 Qualitative imaging variable correlates for WHO grade

Imaging associations with WHO 2019 Grade					
Imaging variable	Total ($n=119$)	1 ($n=47$)	2 ($n=64$)	3 ($n=8$)	p value
Size*	2.4 [1.8,3.9]	2.2 [1.5,3.1]	3.2 [1.8,5.0]	2.9 [2.3,3.7]	0.051[b]
Degree of enhancement*					0.002[c]
Hyperenhancing	61 (53.0)	34 (73.9)	26 (42.6)	1 (12.5)	
Hypoenhancing	28 (24.3)	4 (8.7)	20 (32.8)	4 (50.0)	
Isoenhancing	26 (22.6)	8 (17.4)	15 (24.6)	3 (37.5)	
Uniformity of enhancement*					0.37[c]
Hetero	66 (57.9)	23 (51.1)	37 (60.7)	6 (75.0)	
Homo	48 (42.1)	22 (48.9)	24 (39.3)	2 (25.0)	
Progressive enhancement*					< 0.001[c]
No	74 (75.5)	34 (89.5)	38 (73.1)	2 (25.0)	
Yes	24 (24.5)	4 (10.5)	14 (26.9)	6 (75.0)	
Contours*					0.001[c]
Ill-defined	13 (11.1)	0 (0.0)	10 (15.9)	3 (37.5)	
Lobulated	43 (36.8)	14 (30.4)	25 (39.7)	4 (50.0)	
Rounded	61 (52.1)	32 (69.6)	28 (44.4)	1 (12.5)	
Infiltrative on imaging*					< 0.001[c]
No	98 (83.8)	44 (95.7)	51 (81.0)	3 (37.5)	
Yes	19 (16.2)	2 (4.3)	12 (19.0)	5 (62.5)	
Calcifications*					0.26[c]
No	82 (78.1)	35 (85.4)	42 (75.0)	5 (62.5)	
Yes	23 (21.9)	6 (14.6)	14 (25.0)	3 (37.5)	
Cystic*					0.24[c]
No	80 (72.7)	27 (64.3)	46 (76.7)	7 (87.5)	
Yes	30 (27.3)	15 (35.7)	14 (23.3)	1 (12.5)	
Tumor thrombus*					0.18[d]
No	110 (96.5)	46 (100.0)	56 (93.3)	8 (100.0)	
Yes	4 (3.5)	0 (0.0)	4 (6.7)	0 (0.0)	
Vascular occlusion*					< 0.001[c]
No	96 (83.5)	46 (100.0)	46 (75.4)	4 (50.0)	
Yes	19 (16.5)	0 (0.0)	15 (24.6)	4 (50.0)	
Upstream PD dilatation*					0.005[c]
No	77 (86.5)	37 (92.5)	38 (86.4)	2 (40.0)	
Yes	12 (13.5)	3 (7.5)	6 (13.6)	3 (60.0)	
Upstream atrophy*					0.036[c]
No	72 (81.8)	34 (87.2)	36 (81.8)	2 (40.0)	
Yes	16 (18.2)	5 (12.8)	8 (18.2)	3 (60.0)	

*Data not available for all subjects. Missing values: Size = 1, Degree of enhancement, Uniformity of enhancement, progressive enhancement = 21, Contours = 2, Infiltrative = 2, Calcifications = 14, cystic = 9, Tumor thrombus = 5, Vascular occlusion = 4, Upstream PD dilatation = 30, Upstream atrophy = 31.Values presented as Mean ± SD, Median [P25, P75], Median (min, max) or N (column %).p values: a = ANOVA, b = Kruskal–Wallis test, c = Pearson's chi-square test, d = Fisher's Exact test

absence of cystic components were 3.7 times ($p=0.01$, 95% CI 1.4–10.2) and 3.4 times ($p=0.02$, 95% CI 1.2–10.2) more likely to be associated with MF, respectively. VO was 3.5 times ($p=0.03$, 95%CI 1.1–10.9) more likely to be associated with MF. PD dilatation was 15 times ($p=0.01$, 95%CI 1.7–132.6) more likely to be associated with MF and 42.9 times ($p=0.001$, 95% CI 4.5–410.7) more likely to be associated with IMF. Atrophy was 4.2 times ($p=0.03$, 95% CI 1.1–16.2) more likely to be associated with MF and 9.8 times ($p=0.003$, 95% CI 2.2–43.9) more likely to be associated with IMF.

Table 3 Logistic regression analyses of WHO grade, LVI, and growth pattern by imaging feature

Histopathology feature	Imaging feature	Odds ratio	Lower 95% CI	Upper 95% CI	*p* value
WHO grade[A]	Hypoenhancement[a]	6.96	2.54	19.08	0.0002
	Isoenhancement[a]	3.29	1.28	8.47	0.0134
	Progressive enhancement	6.16	2.14	17.78	0.0008
	Ill-defined contour[b]	15.59	3.77	64.41	0.0001
	Lobulated contour[b]	2.59	1.17	5.75	0.0193
	$Infiltrative_{im}$	8.98	2.7	29.66	0.0003
	PD dilatation	4.74	1.27	17.72	0.0208
	Vascular occlusion	12.46	3.48	44.65	0.0001
LVI[B]	Size	1.21	1.06	1.38	0.0050
	Hypoenhancement[a]	3.03	1.26	7.32	0.0135
	Heterogeneous enhancement	3.88	1.76	8.57	0.0008
	Progressive enhancement	4.46	1.75	11.33	0.0017
	Ill-defined contour[b]	18.00	4.39	73.82	< 0.0001
	Lobulated contour[b]	4.50	1.94	10.46	0.0005
	$Infiltrative_{im}$	25.88	5.67	118.08	< 0.0001
	PD dilatation	4.65	1.41	15.29	0.0114
	Cystic components	3.84	1.45	10.22	0.0070
	Vascular occlusion	51.07	6.54	398.63	0.0002
	Upstream atrophy	7.37	2.49	21.84	0.0003
Infiltrative growth pattern[B]	Hypoenhancement[a]	5.60	1.81	17.31	0.0028
	Isoenhancement[a]	3.38	1.01	11.31	0.0485
	Progressive enhancement	7.68	2.71	21.80	0.0001
	Ill-defined contour[b]	51.33	9.14	288.37	< 0.0001
	$Infiltrative_{im}$	17.33	5.47	54.89	< 0.0001
	PD dilatation	7.39	1.99	27.50	0.0028
	Vascular occlusion	16.94	5.35	53.66	< 0.0001
	Upstream atrophy	4.36	1.27	15.03	0.0196

[A]Ordinal logistic regression. Likelihood ratio corresponds to each stepwise increase in grade from WHO grade 1

[B]Logistic regression

[a]Compared to hyperenhancing

[b]Compared to rounded contour

$Infiltrative_{im}$ = infiltrative imaging appearance

PD = pancreatic duct

CI = confidence interval

Recurrence-free survival

Univariate cox regression analyses for imaging variables show that $infiltrative_{im}$ ($p < 0.001$, HR 6.1 95% CI 2.66–13.81), heterogeneous enhancement ($p = 0.0064$, HR 4.48, 95% CI 1.52–13.16), $enhancement_{prog}$ ($p = 0.0003$, HR 4.53, 95% CI 2.0–10.26), $contour_{ill}$ ($p < 0.001$, HR 25.9, 95%CI 5.57–120.4), lobulated contours ($p = 0.007$, HR 7.82, 95% CI 1.75–34.95), and VO ($p < 0.001$, HR 5.85, 95% CI 2.58–13.27) are associated with an increased hazard of RFS (Table 8). Multivariable analyses of only imaging variables identified $enhancement_{prog}$ ($p = 0.01$, HR 3.02, 95%CI 1.28–7.11) and $contour_{ill}$ ($p = 0.0003$, HR 18.29, 95% CI 3.83–87.3) or lobulated contours ($p = 0.02$, HR 5.3, 95% CI 1.2–26.7) to be associated with an increased hazard of RFS. When considering both pathological and imaging variables, infiltrative growth pattern ($p = 0.003$, HR 4.59, 95% CI 1.68–12.56) and LVI ($p = 0.008$, HR 6.45, 95% CI 1.68–24.78) were found to be associated with an increased hazard of RFS.

Table 4 Qualitative imaging variable correlates for lymphovascular invasion

Imaging associations of lymphovascular invasion				
Imaging variables	Total (N = 131)	No (N = 83)	Yes (N = 48)	*p* value
Size*	2.4 [1.8,3.9]	2.1 [1.5,3.6]	3.2 [2.3,5.4]	0.001[b]
Degree of enhancement*				0.028[c]
Hyper	67 (52.8)	46 (58.2)	21 (43.8)	
Hypo	31 (24.4)	13 (16.5)	18 (37.5)	
Iso	29 (22.8)	20 (25.3)	9 (18.8)	
Uniformity of enhancement*				< 0.001[c]
Hetero	70 (55.6)	34 (43.6)	36 (75.0)	
Homo	56 (44.4)	44 (56.4)	12 (25.0)	
Progressive enhancement*				0.001[c]
No	84 (76.4)	59 (86.8)	25 (59.5)	
Yes	26 (23.6)	9 (13.2)	17 (40.5)	
Contours*				< 0.001[c]
Ill-defined	15 (11.6)	3 (3.7)	12 (25.0)	
Lobulated	48 (37.2)	24 (29.6)	24 (50.0)	
Rounded	66 (51.2)	54 (66.7)	12 (25.0)	
Infiltrative on imaging*				< 0.001[c]
No	108 (83.7)	79 (97.5)	29 (60.4)	
Yes	21 (16.3)	2 (2.5)	19 (39.6)	
Calcifications*				0.73[c]
No	90 (78.9)	56 (80.0)	34 (77.3)	
Yes	24 (21.1)	14 (20.0)	10 (22.7)	
Cystic components*				0.005[c]
No	89 (73.0)	48 (64.0)	41 (87.2)	
Yes	33 (27.0)	27 (36.0)	6 (12.8)	
Tumor thrombus*				0.069[d]
No	121 (96.0)	77 (98.7)	44 (91.7)	
Yes	5 (4.0)	1 (1.3)	4 (8.3)	
Vascular occlusion*				< 0.001[c]
No	107 (84.3)	78 (98.7)	29 (60.4)	
Yes	20 (15.7)	1 (1.3)	19 (39.6)	
Upstream PD dilatation*				0.007[c]
No	86 (86.0)	62 (92.5)	24 (72.7)	
Yes	14 (14.0)	5 (7.5)	9 (27.3)	
Upstream atrophy*				< 0.001[c]
No	79 (79.8)	60 (90.9)	19 (57.6)	
Yes	20 (20.2)	6 (9.1)	14 (42.4)	

*Data not available for all subjects. Missing values: Size = 2, Degree of enhancement, Uniformity of enhancement, and Progressive enhancement = 21, Contours = 2, Infiltrative = 2, calcifications = 17, cystic = 1, Tumor Thrombus = 5, Vascular Occlusion = 4, Upstream PD dilatation = 31, Upstream Atrophy = 32. Values presented as Mean ± SD, Median [P25, P75], or N (column %). p values: a = ANOVA, b = Kruskal–Wallis test, c = Pearson's chi-square test, d = Fisher's Exact test

Overall survival

Imaging variables associated with OS were infiltrative$_{im}$ ($p = 0.032$, HR 3, 95% CI 1.1–8.11), contour$_{ill}$ ($p = 0.02$, HR 5.46, 95% CI 1.29–23.13), and VO ($p = 0.001$, HR 5.39, 95% CI 1.99–14.61) (Table 8). When considering only imaging variables, older age at diagnosis ($p = 0.01$, HR 1.058, 95% CI 1.01–1.108) and VO ($p = 0.0004$, HR 6.08, 95% CI 2.22–16.68) were associated with increased hazard to OS. When considering both pathological and imaging variables, only older age at diagnosis ($p = 0.007$, HR 1.08, 95%CI 1.02–1.137) and LVI ($p = 0.008$, HR 13.9, 95% CI 3.00–64.48) were found to be associated with an increased hazard of OS.

Table 5 Qualitative imaging variable correlates for growth pattern

Imaging associations of growth pattern				
Imaging variable	Total ($N=120$)	Circumscribed ($N=96$)	Infiltrative ($N=24$)	p value
Size*	2.4 [1.8,3.9]	2.4 [1.7,3.9]	2.7 [1.9,4.6]	0.51[b]
Degree of enhancement*				0.006[c]
Hyper	61 (52.6)	55 (59.8)	6 (25.0)	
Hypo	29 (25.0)	18 (19.6)	11 (45.8)	
Iso	26 (22.4)	19 (20.7)	7 (29.2)	
Uniformity of enhancement*				0.92[c]
Hetero	66 (57.4)	52 (57.1)	14 (58.3)	
Homo	49 (42.6)	39 (42.9)	10 (41.7)	
Progressive enhancement*				< 0.001[c]
No	75 (75.8)	65 (85.5)	10 (43.5)	
Yes	24 (24.2)	11 (14.5)	13 (56.5)	
Contours*				< 0.001[c]
Ill-defined	13 (11.0)	2 (2.1)	11 (45.8)	
Lobulated	43 (36.4)	36 (38.3)	7 (29.2)	
Rounded	62 (52.5)	56 (59.6)	6 (25.0)	
Infiltrative on imaging*				< 0.001[c]
No	99 (83.9)	88 (93.6)	11 (45.8)	
Yes	19 (16.1)	6 (6.4)	13 (54.2)	
Calcifications*				0.65[c]
No	83 (78.3)	65 (77.4)	18 (81.8)	
Yes	23 (21.7)	19 (22.6)	4 (18.2)	
Cystic*				0.070[c]
No	81 (73.0)	60 (69.0)	21 (87.5)	
Yes	30 (27.0)	27 (31.0)	3 (12.5)	
Tumor Thrombus*				0.19[d]
No	111 (96.5)	89 (97.8)	22 (91.7)	
Yes	4 (3.5)	2 (2.2)	2 (8.3)	
Vascular Occlusion*				< 0.001[c]
No	97 (83.6)	86 (93.5)	11 (45.8)	
Yes	19 (16.4)	6 (6.5)	13 (54.2)	
Upstream PD dilatation*				< 0.001[c]
No	77 (85.6)	69 (90.8)	8 (57.1)	
Yes	13 (14.4)	7 (9.2)	6 (42.9)	
Upstream Atrophy*				0.014[c]
No	72 (80.9)	64 (85.3)	8 (57.1)	
Yes	17 (19.1)	11 (14.7)	6 (42.9)	

*Data not available for all subjects. Missing values: Size = 2, Degree of enhancement, heterogeneity of enhancement, progressive enhancement = 21, Contours = 2, Infiltrative = 2, Upstream PD dilatation = 30, calcifications = 14, cystic = 9, Tumor Thrombus = 5, Vascular Occlusion = 4, Upstream Atrophy = 31. Values presented as Mean ± SD, Median [P25, P75], Median (min, max) or N (column %). p values: a = ANOVA, b = Kruskal–Wallis test, c = Pearson's chi-square test, d = Fisher's Exact test

Discussion

The goal was to determine if histopathologic features of PanNEN linked to patient outcome (WHO grade, LVI, growth pattern, and intratumoral fibrosis) have qualitative correlates on preoperative imaging. We found three imaging features associated with all four histopathologic parameters and patient outcome (RFS HR ranging from 5.8 to 25.9 and OS HR ranging from 3 to 5.5). These features are (1) infiltrative$_{im}$, (2) contour$_{ill}$, and (3) VO. We found that grade 3 tumors were up to 30 times more likely than grade 1 tumors to show contour$_{ill}$ ($p = 0.0001$). PanNEN with VO were 51.1 times ($p = 0.0002$) more likely to demonstrate LVI. PanNEN with contour$_{ill}$ were 51.3 times ($p < 0.0001$) more likely to show infiltrative histopathologic growth pattern and 14 times ($p = 0.0065$) more likely to show fibrosis.

Table 6 Qualitative imaging variable correlates for intratumoral fibrosis

Imaging associations for intratumoral fibrosis					
Factor	Total ($N=120$)	No Fibrosis ($N=70$)	Mature Fibrosis ($N=36$)	Immature Fibrosis ($N=14$)	p value
Size*	2.4 [1.8,3.9]	2.4 [1.8,4.1]	2.9 [1.8,4.0]	2.3 [1.5,3.8]	0.77[b]
Degree of enhancement*					0.006[c]
Hyper	61 (52.6)	38 (56.7)	19 (54.3)	4 (28.6)	
Hypo	29 (25.0)	11 (16.4)	14 (40.0)	4 (28.6)	
Iso	26 (22.4)	18 (26.9)	2 (5.7)	6 (42.9)	
Uniformity of enhancement*					0.34[c]
Hetero	66 (57.4)	36 (53.7)	23 (67.6)	7 (50.0)	
Homo	49 (42.6)	31 (46.3)	11 (32.4)	7 (50.0)	
Progressive enhancement*					0.048[c]
No	75 (75.8)	48 (82.8)	21 (72.4)	6 (50.0)	
Yes	24 (24.2)	10 (17.2)	8 (27.6)	6 (50.0)	
Contours*					0.010[c]
Ill-defined	13 (11.0)	2 (2.9)	7 (20.0)	4 (28.6)	
Lobulated	43 (36.4)	25 (36.2)	14 (40.0)	4 (28.6)	
Rounded	62 (52.5)	42 (60.9)	14 (40.0)	6 (42.9)	
Infiltrative*					< 0.001[c]
No	99 (83.9)	65 (94.2)	26 (74.3)	8 (57.1)	
Yes	19 (16.1)	4 (5.8)	9 (25.7)	6 (42.9)	
Calcifications*					0.024[c]
No	83 (78.3)	53 (85.5)	19 (61.3)	11 (84.6)	
Yes	23 (21.7)	9 (14.5)	12 (38.7)	2 (15.4)	
Cystic components*					0.013[c]
No	81 (73.0)	40 (62.5)	29 (85.3)	12 (92.3)	
Yes	30 (27.0)	24 (37.5)	5 (14.7)	1 (7.7)	
Tumor thrombus*					0.76[d]
No	111 (96.5)	65 (97.0)	32 (94.1)	14 (100.0)	
Yes	4 (3.5)	2 (3.0)	2 (5.9)	0 (0.0)	
Vascular occlusion*					0.040[c]
No	97 (83.6)	61 (91.0)	26 (74.3)	10 (71.4)	
Yes	19 (16.4)	6 (9.0)	9 (25.7)	4 (28.6)	
Upstream PD dilatation*					< 0.001[c]
No	77 (85.6)	50 (98.0)	20 (76.9)	7 (53.8)	
Yes	13 (14.4)	1 (2.0)	6 (23.1)	6 (46.2)	
Upstream atrophy*					0.004[c]
No	72 (80.9)	46 (92.0)	19 (73.1)	7 (53.8)	
Yes	17 (19.1)	4 (8.0)	7 (26.9)	6 (46.2)	

*Data not available for all subjects. Missing values: Size = 1, Degree of enhancement, Uniformity of enhancement, Progressive enhancement = 21, Contours = 2, Infiltrative = 2, Upstream PD dilatation = 30, calcifications = 14, cystic = 9, Tumor Thrombus = 5, Vascular Occlusion = 4, Upstream Atrophy = 31. Values presented as Mean ± SD, Median [P25, P75], Median (min, max) or N (column %). p values: a = ANOVA, b = Kruskal–Wallis test, c = Pearson's chi-square test, d = Fisher's Exact test

Our findings regarding the poor prognostic sign of $\text{contour}_{\text{ill}}$ [11, 12] and infiltrative imaging appearance [13, 14] are consistent with other studies. Likewise, the association of VO with aggressive tumor biology in our study is consistent with prior reports [11, 15–17]. However, our study goes beyond WHO grade (based on tumor differentiation and ki-67 index) and shows that these qualitative imaging features also reflect LVI, infiltrative growth pattern, and intratumoral fibrosis, all aggressive features of PanNEN on histopathology.

There is mounting evidence that fibrosis in PanNEN is associated with more aggressive disease [3, 9, 10, 18]. Studies on tumor enhancement have had limited success in identifying fibrosis [9] and as in our study morphologic assessment on imaging may better reflect fibrosis. We

Table 7 Multivariable logistic regression analyses for intratumoral fibrosis

	Mature fibrosis				Immature fibrosis			
Imaging feature	Odds ratio	Lower 95% CI	Upper 95% CI	*p*- value	Odds ratio	Lower 95% CI	Upper 95% CI	*p*- value
Hypoenhancement[a]	11.45	2.18	60.28	0.0040	–	–	–	0.9077
Progressive enhancement	–	–	–	0.2652	4.80	1.28	17.99	0.0199
Ill-defined contour[b]	10.5	1.95	56.55	0.0062	14.0	2.09	93.67	0.0065
Ill-defined contour[c]	6.25	1.14	34.29	0.0349	12.5	1.69	92.25	0.0133
$Infiltrative_{im}$	5.62	1.59	19.87	0.0073	12.18	2.82	52.60	0.0008
Calcifications	3.72	1.35	10.22	0.0109	–	–	–	0.9359
No cystic components	3.48	1.19	10.20	0.0231	–	–	–	0.0656
Vascular occlusion	3.52	1.14	10.90	0.0291	–	–	–	0.0547
PD dilatation	15.0	1.70	132.64	0.0149	42.86	4.47	410.68	0.0011
Upstream atrophy	4.24	1.1	16.17	0.0347	9.86	2.21	43.91	0.0027

[a]Compared to isoenhancing

[b]Compared to rounded contour

[c]Compared to lobulated contour

$Infiltrative_{im}$ = infiltrative imaging appearance

PD = pancreatic duct

CI = confidence interval

Table 8 Univariate Cox Regression Analysis for RFS and OS

Imaging variable	RFS				OS			
	HR	Lower 95% CI	Upper 95% CI	P	HR	Lower 95% CI	Upper 95% CI	*P*
Infiltrative appearance	6.063	2.661	13.814	< .0001	2.985	1.099	8.110	0.0320
Hyperenhancement	0.813	0.258	2.563	0.7240	0.904	0.240	3.413	0.8817
Hypoenhancement	2.812	0.976	8.106	0.0556	2.165	0.632	7.417	0.2190
Heterogeneous enhancement	4.477	1.523	13.164	0.0064	2.923	0.830	10.295	0.0950
Progressive enhancement	4.525	1.996	10.259	0.0003	2.215	0.799	6.141	0.1263
Ill-defined contours	25.897	5.570	120.404	< .0001	5.464	1.291	23.132	0.0211
Lobulated contours	7.822	1.751	34.954	0.0071	2.882	0.760	10.921	0.1195
PD dilatation	2.151	0.797	5.802	0.1304	1.503	0.423	5.341	0.5292
Calcifications	1.344	0.497	3.636	0.5600	2.713	0.801	9.191	0.1089
Cystic components	0.972	0.359	2.632	0.9562	1.164	0.323	4.191	0.8161
Tumor thrombus	3.557	0.832	15.201	0.0869	2.444	0.315	18.949	0.3926
Vascular occlusion	5.846	2.576	13.267	< .0001	5.392	1.990	14.611	0.0009
Upstream atrophy	1.407	0.522	3.794	0.4997	1.560	0.500	4.861	0.4434
Size	1.094	0.978	1.224	0.1163	0.997	0.851	1.168	0.9730

found that IMF in particular was associated with $contour_{ill}$, $infiltrative_{im}$, PD dilatation, and atrophy, all imaging features associated with higher grade tumor. IMF was nearly 43 times and MF was 15 times more likely to be associated with PD dilatation. PD dilatation has been shown to be associated with fibrosis [9, 19] and poorer prognosis [11, 14, 20]. Studies examining the significance of fibrosis in PanNEN, thus, far have not distinguished between MF and IMF [3, 9, 10, 18, 21–23]. IMF more closely resembles desmoplastic reaction that is commonly seen with aggressive and rapidly growing neoplasms such as pancreatic ductal adenocarcinoma. This is in contrast to the hypocellular hyalinized stroma in MF that is seen mostly in benign and slow-growing lesions [24]. Future investigations may benefit from distinguishing between MF and IMF. For example, calcifications in PanNEN were significantly associated with MF but not IMF in our study. Although some prior studies linked calcification to aggressive panNEN [14, 25, 26], others did not [11–13, 27], raising question about the nature of the underlying fibrosis in these populations. Dystrophic calcifications commonly occur in long-standing fibrosis and hyalinization of stroma involving slow-growing benign neoplasms [24] or reactive/

inflammatory conditions such as calcified granulomas and arteriosclerosis. While most PanNEN are cellular tumors with scant stroma, a subset of these tumors incites a reaction which leads to mature collagen deposition, in turn allowing for the development of dystrophic calcification.

Tumor size was associated only with LVI, and no other histopathologic parameter, including WHO grade in this surgically managed cohort. Currently, the guidelines for PanNEN management are mostly driven by threshold tumor size of 2 cm for surgical intervention [28, 29]. Our results show that size alone may be inadequate for preoperative determination of tumor aggression. Future prospective investigation of sub-2 cm PanNEN for these imaging features could be considered.

For the practicing radiologist, the results of this study also demonstrate the wide spectrum of imaging appearances for surgically managed PNEN; nearly half of PNEN do not hyperenhance, more than half demonstrate heterogeneous enhancement, more than half deviate from a round contour, and more than a quarter have cystic components. Furthermore, more than 15% can result in vascular occlusion and 3.5% demonstrate contiguous tumor thrombus. These results add to the growing data reflecting a *spectrum* of imaging appearance for PNEN rather than categorization of the appearances as "typical" and "atypical." The results of this paper show that there are histologic and prognostic correlate to this spectrum of imaging appearances.

There are some limitations to our study. First, there was no standardized imaging modality for inclusion, as we wished to include the largest number of cases to assess as many imaging features as possible. However, both contrast-enhanced CT and MR reflect enhancement and tumor morphology in a similar fashion, and current National Comprehensive Cancer Network guidelines, for example, do not distinguish between the 2 modalities [30]. CT has advantage in detecting tumor calcification, whereas cystic components are more confidently appreciated on MR. Second, while many CTs were scanned according to pancreas protocol, there was no standardized scanning protocol for the images acquired at an outside facility. Therefore, our assessment and conclusions particularly regarding enhancement may not be as robust compared to studies with standardized pancreatic imaging. We attempted to control for this as best as possible, by using background pancreatic enhancement as an internal control. It should be noted that only 3 of the 12 imaging features were directly related to assessment of enhancement, whereas the remaining 9 features were not dependent on the timing of post-contrast image acquisition. Furthermore, being inclusive of a heterogeneous pool of imaging studies is probably more reflective of true clinical practice at a PanNEN referral center and our study shows that prognostic qualitative imaging features can be appreciated through this "noise." A third limitation pertains to population size and selection bias. Given the relative infrequency of PanNEN, the number of cases is reasonable and on par with similar studies. We included only surgically managed patients, implying tumor localized to the pancreas and patients fit for surgery. Therefore, the imaging features of aggressive, metastatic PanNEN are probably underrepresented. Likewise, tumors smaller than 2 cm are probably also underrepresented since 2 cm is the threshold for surgical management [28, 29]. We also excluded patients with multifocal PanNEN, and therefore, syndromic tumors, but this is probably appropriate as some authors believe that these tumors to be clinically distinct from sporadic PanNEN [31], and multifocality may not enable confident radiologic-pathologic correlation.

Our results show that prognostication of tumor biology can be extracted by the radiologist from routine, clinically acquired CT and MR images, and should be reported. These qualitative imaging features will probably be most helpful in the preoperative management of tumors. There are several potential clinical scenarios: (1) Determine concordance with biopsy specimens. Tumor undersampling, particularly in heterogeneous tumors, may histologically give the false impression of a low-grade tumor. Evaluation for imaging concordance may better inform the patient care team's impression of tumor biology. (2) Determine if surgical management is appropriate for sub-2 cm tumors. Current surgical guidelines recommend resection for tumors larger than 2 cm [28, 29]. Sallinen et al. [20] showed that the presence of ductal dilatation in sub- 2 cm tumors may warrant surgical management. We also evaluated ductal dilatation but found that other imaging features like infiltrative$_{im}$, contour$_{ill}$, and VO were associated with patient outcome. Evaluation for these features may, therefore, be helpful to expedite surgical management of sub-2 cm tumors. (3) Guide the need for additional imaging prior to surgical management. The presence of aggressive imaging features may increase suspicion for metastatic disease that is occult on conventional imaging. Examinations such as somatostatin receptor imaging (i.e., DOTATATE PET) or liver MRI may be more valuable in these patients to accurately stage disease. Likewise, tumors without aggressive imaging features may be able to forgo additional preoperative imaging workup. (4) Inform the extent of surgical lymphadenectomy at the time of PanNEN resection. More aggressive tumors are more likely to harbor micrometastatic disease in lymph nodes that are not pathologically enlarged on imaging and more extensive nodal dissection may prove helpful. (5) Provide a window of opportunity to evaluate novel treatment paradigms prior to surgical management. For example, one could investigate the role of neoadjuvant therapy in the long-term outcomes of patients with more aggressive tumors.

Preoperative CT or MR, obtained in nearly all patients, provides readily available qualitative information about the underlying histopathologic features of PanNEN. Assessment

for infiltrative$_{im}$, contour$_{ill}$, and VO, in particular, may best inform tumor biology.

Funding None.

References

1. Taskin, O.C., C.N. Clarke, M. Erkan, S. Tsai, D.B. Evans, and V. Adsay, (2020) Pancreatic neuroendocrine neoplasms: current state and ongoing controversies on terminology, classification and prognostication. J Gastrointest Oncol. 11(3): p. 548-558 DOI: https://doi.org/10.21037/jgo.2020.03.07.
2. Chatterjee, D., N.A. Trikalinos, G.A. Williams, J. Liu, W.G. Hawkins, and C. Hammill, (2020) Intratumoral Fibrosis and Tumor Growth Pattern as Prognostic Factors in Optimally Resected Pancreatic Neuroendocrine Neoplasms: An Analysis of 168 Cases. Pancreas. 49(2): p. 255-260 DOI: https://doi.org/10.1097/MPA.0000000000001478.
3. Johnson, A., J.P. Wright, Z. Zhao, T. Komaya, A. Parikh, N. Merchant, and C. Shi, (2015) Cadherin 17 is frequently expressed by 'sclerosing variant' pancreatic neuroendocrine tumour. Histopathology. 66(2): p. 225-33 DOI: https://doi.org/10.1111/his.12535.
4. Paiella, S., L. Landoni, R. Rota, M. Valenti, G. Elio, S.F. Crino, E. Manfrin, A. Parisi, S. Cingarlini, M. D'Onofrio, A. Scarpa, R.T. Lawlor, L. Bernardoni, P. Capelli, C. Nessi, M. Miotto, A. Gabbrielli, C. Bassi, and R. Salvia, (2020) Endoscopic ultrasound-guided fine-needle aspiration for the diagnosis and grading of pancreatic neuroendocrine tumors: a retrospective analysis of 110 cases. Endoscopy DOI: https://doi.org/10.1055/a-1180-8614.
5. Hwang, H.S., Y. Kim, S. An, S.J. Kim, J.Y. Kim, S.Y. Kim, D.W. Hwang, D.H. Park, S.S. Lee, S.C. Kim, D.W. Seo, and S.M. Hong, (2018) Grading by the Ki-67 Labeling Index of Endoscopic Ultrasound-Guided Fine Needle Aspiration Biopsy Specimens of Pancreatic Neuroendocrine Tumors Can Be Underestimated. Pancreas. 47(10): p. 1296-1303 DOI: https://doi.org/10.1097/MPA.0000000000001157.
6. Lee, N.J., R.H. Hruban, and E.K. Fishman, (2018) Pancreatic neuroendocrine tumor: review of heterogeneous spectrum of CT appearance. Abdom Radiol (NY). 43(11): p. 3025-3034 DOI: https://doi.org/10.1007/s00261-018-1574-4.
7. Rodallec, M., V. Vilgrain, A. Couvelard, P. Rufat, D. O'Toole, V. Barrau, A. Sauvanet, P. Ruszniewski, and Y. Menu, (2006) Endocrine pancreatic tumours and helical CT: contrast enhancement is correlated with microvascular density, histoprognostic factors and survival. Pancreatology. 6(1-2): p. 77-85 DOI: https://doi.org/10.1159/000090026.
8. d'Assignies, G., A. Couvelard, S. Bahrami, M.P. Vullierme, P. Hammel, O. Hentic, A. Sauvanet, P. Bedossa, P. Ruszniewski, and V. Vilgrain, (2009) Pancreatic endocrine tumors: tumor blood flow assessed with perfusion CT reflects angiogenesis and correlates with prognostic factors. Radiology. 250(2): p. 407-16 DOI: https://doi.org/10.1148/radiol.2501080291.
9. Kim, C., J.H. Byun, S.M. Hong, S. An, J.H. Kim, S.S. Lee, and H.J. Kim, (2017) A comparison of enhancement patterns on dynamic enhanced CT and survival between patients with pancreatic neuroendocrine tumors with and without intratumoral fibrosis. Abdom Radiol (NY). 42(12): p. 2835-2842 DOI: https://doi.org/10.1007/s00261-017-1212-6.
10. Yano, M., S. Misra, D.H. Carpenter, A. Salter, and C.F. Hildebolt, (2017) Pancreatic Neuroendocrine Tumors: Computed Tomography Enhancement, But Not Histological Grade, Correlates With Tumor Aggression. Pancreas. 46(10): p. 1366-1372 DOI: https://doi.org/10.1097/MPA.0000000000000922.
11. Choi, T.W., J.H. Kim, M.H. Yu, S.J. Park, and J.K. Han, (2018) Pancreatic neuroendocrine tumor: prediction of the tumor grade using CT findings and computerized texture analysis. Acta Radiol. 59(4): p. 383-392 DOI: https://doi.org/10.1177/0284185117725367.
12. Yang, B., H.Y. Chen, X.Y. Zhang, Y. Pan, Y.F. Lu, and R.S. Yu, (2020) The prognostic value of multidetector CT features in predicting overall survival outcomes in patients with pancreatic neuroendocrine tumors. Eur J Radiol. 124: p. 108847 DOI: https://doi.org/10.1016/j.ejrad.2020.108847.
13. Salahshour, F., M.M. Mehrabinejad, A. Zare Dehnavi, A. Alibakhshi, H. Dashti, M.A. Ataee, and N. Ayoobi Yazdi, (2020) Pancreatic neuroendocrine tumors (pNETs): the predictive value of MDCT characteristics in the differentiation of histopathological grades. Abdom Radiol (NY) DOI: https://doi.org/10.1007/s00261-019-02372-x.
14. Li, W.X., F. Miao, X.Q. Xu, J. Zhang, Z.Y. Wu, K.M. Chen, F.H. Yan, and X.Z. Lin, (2020) Pancreatic Neuroendocrine Neoplasms: CT Spectral Imaging in Grading. Acad Radiol DOI: https://doi.org/10.1016/j.acra.2020.01.033.
15. Bian, Y., Z. Zhao, H. Jiang, X. Fang, J. Li, K. Cao, C. Ma, S. Guo, L. Wang, G. Jin, J. Lu, and J. Xu, (2020) Noncontrast Radiomics Approach for Predicting Grades of Nonfunctional Pancreatic Neuroendocrine Tumors. J Magn Reson Imaging DOI: https://doi.org/10.1002/jmri.27176.
16. Canellas, R., K.S. Burk, A. Parakh, and D.V. Sahani, (2018) Prediction of Pancreatic Neuroendocrine Tumor Grade Based on CT Features and Texture Analysis. AJR Am J Roentgenol. 210(2): p. 341-346 DOI: https://doi.org/10.2214/AJR.17.18417.
17. Kato, T., A. Kudo, Y. Kinowaki, Y. Ishikawa, S. Watanabe, K. Akahoshi, K. Ogawa, H. Ono, D. Ban, S. Tanaka, and M. Tanabe, (2021) A novel classification of portal venous tumor invasion to predict residual tumor status after surgery in patients with pancreatic neuroendocrine neoplasms. J Cancer Res Clin Oncol DOI: https://doi.org/10.1007/s00432-021-03660-0.
18. Tatsumoto, S., Y. Kodama, Y. Sakurai, T. Shinohara, A. Katanuma, and H. Maguchi, (2013) Pancreatic neuroendocrine neoplasm: correlation between computed tomography enhancement patterns and prognostic factors of surgical and endoscopic ultrasound-guided fine-needle aspiration biopsy specimens. Abdom Imaging. 38(2): p. 358-66 DOI: https://doi.org/10.1007/s00261-012-9953-8.
19. Shi, C., S.S. Siegelman, S. Kawamoto, C.L. Wolfgang, R.D. Schulick, A. Maitra, and R.H. Hruban, (2010) Pancreatic duct stenosis secondary to small endocrine neoplasms: a manifestation of serotonin production? Radiology. 257(1): p. 107-14 DOI: https://doi.org/10.1148/radiol.10100046.
20. Sallinen, V., C. Haglund, and H. Seppanen, (2015) Outcomes of resected nonfunctional pancreatic neuroendocrine tumors: Do size and symptoms matter? Surgery. 158(6): p. 1556-63 DOI: https://doi.org/10.1016/j.surg.2015.04.035.
21. Takaji, R., S. Matsumoto, H. Mori, Y. Yamada, N. Hongo, S. Tanoue, M. Ota, S. Kitano, and K. Fukuzawa, (2009) Carcinoid tumors of the pancreas: dynamic CT and MRI features with pathological correlation. Abdom Imaging. 34(6): p. 753-8 DOI: https://doi.org/10.1007/s00261-008-9470-y.
22. Wang, Y., Z.E. Chen, V. Yaghmai, P. Nikolaidis, R.J. McCarthy, L. Merrick, and F.H. Miller, (2011) Diffusion-weighted MR imaging in pancreatic endocrine tumors correlated with histopathologic characteristics. J Magn Reson Imaging. 33(5): p. 1071-9 DOI: https://doi.org/10.1002/jmri.22541.

23. McCall, C.M., C. Shi, A.P. Klein, B. Konukiewitz, B.H. Edil, T.A. Ellison, C.L. Wolfgang, R.D. Schulick, G. Kloppel, and R.H. Hruban, (2012) Serotonin expression in pancreatic neuroendocrine tumors correlates with a trabecular histologic pattern and large duct involvement. Hum Pathol. 43(8): p. 1169-76 DOI: https://doi.org/10.1016/j.humpath.2011.09.014.
24. Chorti, A., T.S. Papavramidis, and A. Michalopoulos, (2016) Calcifying Fibrous Tumor: Review of 157 Patients Reported in International Literature. Medicine (Baltimore). 95(20): p. e3690 DOI: https://doi.org/10.1097/MD.0000000000003690.
25. Poultsides, G.A., L.C. Huang, Y. Chen, B.C. Visser, R.K. Pai, R.B. Jeffrey, W.G. Park, A.M. Chen, P.L. Kunz, G.A. Fisher, and J.A. Norton, (2012) Pancreatic neuroendocrine tumors: radiographic calcifications correlate with grade and metastasis. Ann Surg Oncol. 19(7): p. 2295-303 DOI: https://doi.org/10.1245/s10434-012-2305-7.
26. McGovern, J.M., A.D. Singhi, A.A. Borhani, A. Furlan, K.M. McGrath, H.J. Zeh, 3rd, N. Bahary, and A.K. Dasyam, (2018) CT Radiogenomic Characterization of the Alternative Lengthening of Telomeres Phenotype in Pancreatic Neuroendocrine Tumors. AJR Am J Roentgenol. 211(5): p. 1020-1025 DOI: https://doi.org/10.2214/AJR.17.19490.
27. D'Onofrio, M., V. Ciaravino, N. Cardobi, R. De Robertis, S. Cingarlini, L. Landoni, P. Capelli, C. Bassi, and A. Scarpa, (2019) CT Enhancement and 3D Texture Analysis of Pancreatic Neuroendocrine Neoplasms. Sci Rep. 9(1): p. 2176 DOI: https://doi.org/10.1038/s41598-018-38459-6.
28. Howe, J.R., N.B. Merchant, C. Conrad, X.M. Keutgen, J. Hallet, J.A. Drebin, R.M. Minter, T.C. Lairmore, J.F. Tseng, H.J. Zeh, S.K. Libutti, G. Singh, J.E. Lee, T.A. Hope, M.K. Kim, Y. Menda, T.R. Halfdanarson, J.A. Chan, and R.F. Pommier, (2020) The North American Neuroendocrine Tumor Society Consensus Paper on the Surgical Management of Pancreatic Neuroendocrine Tumors. Pancreas. 49(1): p. 1-33 DOI: https://doi.org/10.1097/MPA.0000000000001454.
29. Falconi, M., D.K. Bartsch, B. Eriksson, G. Kloppel, J.M. Lopes, J.M. O'Connor, R. Salazar, B.G. Taal, M.P. Vullierme, D. O'Toole, and p. Barcelona Consensus Conference, (2012) ENETS Consensus Guidelines for the management of patients with digestive neuroendocrine neoplasms of the digestive system: well-differentiated pancreatic non-functioning tumors. Neuroendocrinology. 95(2): p. 120-34 DOI: https://doi.org/10.1159/000335587.
30. Network, N.C.C., (2021) Clinical Practice Guidelines in Oncology, Neuroendocrine and Adrenal Tumors, Version 3.2021.
31. Soczomski, P., B. Jurecka-Lubieniecka, A. Krzywon, A.J. Cortez, S. Zgliczynski, N. Rogozik, M. Oczko-Wojciechowska, A. Pawlaczek, T. Bednarczuk, and B. Jarzab, (2021) A Direct Comparison of Patients With Hereditary and Sporadic Pancreatic Neuroendocrine Tumors: Evaluation of Clinical Course, Prognostic Factors and Genotype-Phenotype Correlations. Front Endocrinol (Lausanne). 12: p. 681013 DOI: https://doi.org/10.3389/fendo.2021.681013.